Molecular-dynamics simulations of shock-induced detonations in solids

S. G. Lambrakos, M. Peyrard,* E. S. Oran, and J. P. Boris
Laboratory for Computational Physics and Fluid Dynamics, Naval Research Laboratory, Washington, D.C. 20375-5000
(Received 9 May 1988)

We present an approach to investigating the propagation of shock-induced detonations in three-dimensional energetic crystals based on a model separating intramolecular and intermolecular motions and new algorithms for tracking particles (the monotonic Lagrangian grid algorithm) and for maintaining constraints among particles (the adaptive constraint algorithm). Separating motions on vastly different time scales allows greater computational efficiency and greater flexibility for modeling the chemical processes. The physical model consists of a three-dimensional lattice in which the intermolecular interactions are given by Lennard-Jones potentials and, under the right conditions, the intramolecular bonds may dissociate and release energy. Calculations of detonations propagating through an explosive show the effects of lattice geometry, energy transfer, and delay time for molecular dissociation.

I. INTRODUCTION

While the understanding of detonations in gases has made tremendous progress in the last few years, the structure of shock-induced detonations in condensed phases, and particularly solids, is far from being understood.[1] Although some underlying mechanisms may be similar in the gas and solid states, a major difference lies in the spatial scale of the phenomena. Recent experiments in fluids[2] suggest that the width of a shock front in a condensed phase is of the order of a few atomic distances, which is in agreement with a theoretical analysis of highly supersonic compressive waves in atomic lattice.[3] Thus, to provide information at the scale of the phenomena involved in the propagation of a detonation wave in a crystal, the studies must be at a microscopic level. Experiments on such small scales are extremely difficult to perform and interpret. Numerical calculations, such as those using molecular-dynamics techniques, can provide a useful complement to the experiments because they can yield extremely detailed information on atomic motions and on the coupling between the different regions that comprise a detonation wave.

Molecular-dynamics studies of shocks in crystal lattices[4-7] have confirmed that the width of a shock in a crystal is of the order of a few unit cells and suggest that the region behind the shock, extending over a distance of many unit cells, is not in thermal equilibrium. Karo *et al.*,[8] who were the first to use molecular dynamics to study detonations in solids, investigated a two-dimensional monatomic crystal consisting of atoms bound to each other by a predissociative exothermic potential. They found that the widths of the induction zone and of the shock front may be of the order of a few unit cells. In a more recent investigation of a model of diatomic molecules embedded in a monatomic lattice, Karo *et al.*[9] showed that a narrow shock front can transmit substantial amounts of energy from intermolecular motions to intramolecular modes.

Recent studies of shock-induced detonations have been carried out by Peyrard *et al.*[10,11] in two-dimensional solids and Tsai and Trevino[12,13] in three-dimensional solids. Tsai and Trevino[12,13] showed that the region behind the shock front is not in thermal equilibrium. However, their model consists of a highly symmetric solid made of one type of atom and one type of bond that is maintained by a predissociative potential. Peyrard *et al.*[10,11] used a more sophisticated lattice model to study how detonation properties depend on the structural characteristics of solids. They modeled an energetic solid that consisted of an array of two-component molecules corresponding to an approximate representation of solid-phase nitromethane. The model consists of three types of intermolecular bonds and a predissociative intramolecular bond, all represented by Morse or Lennard-Jones potentials. Peyrard *et al.*[10] showed that there are conditions on both the geometry of the solid and on the intramolecular and intermolecular potentials that must be met in order to sustain a detonation. In particular, these simulations showed that the energy released from an exothermic chemical reaction is transferred to the shock front through coherent excitation of the crystal lattice; that the reaction front, i.e., the front defined by the onset of molecular dissociation, propagates only if the potentially dissociative bonds link two inequivalent sublattices; and that the energy transfer between longitudinal and transverse motions plays an important role in determining the structure of the detonation.

A study of microscopic detonation structure has to consider the effects of (1) the lattice geometry, unit-cell structure, and interparticle bond strength; (2) the dimensionality of the lattice, i.e., one, two, or three dimensions; (3) the interaction between the different regions that make up a detonation wave, i.e., the nature and role of the transmission of information between these regions; (4) the characteristic response time of potentially dissociative molecules subjected to stress fields in a lattice; and (5) the chemistry of the reaction path from reactants to products.

Previous studies addressed the first three points.

Moreover, because in standard molecular-dynamics calculations all interactions between particles have to be represented by a potential energy, the chemistry of the detonation was included through a predissociative intramolecular potential that allowed, under the appropriate conditions, a classical metastable bond to break. In most of the previous calculations,[8-10,12,13] an exothermic predissociative potential modeled the chemical energy release in a detonation. This approach uses this potential as a model that summarizes the complex chemical reactions that occur in a real energetic material as a simple bond-breaking process. Recent calculations[11] have introduced a two-step chemistry in which the bond breaking, either endothermic or exothermic, is followed by some energy release in the fluid phase behind the shock. However, all chemical processes are still represented by a classical mechanical model.

In this paper we introduce a new approach based on a model for separating the effects of intramolecular and intermolecular motions and on the monotonic Lagrangian grid algorithm for particle tracking[14,15] and the adaptive constraint algorithm.[16] Separating the different time scales which arise because intramolecular modes generally have much higher frequencies than the intermolecular modes is an important problem both computationally and physically. To resolve the fast intramolecular vibrations, the time step used in the computation has to be an order of magnitude smaller than to resolve the intermolecular modes and this results in very expensive calculations. Now, by resolving only the intermolecular motions and modeling the intramolecular motions, the calculation is less expensive and, in addition, we now have the freedom to introduce more sophisticated models for the chemical reactions. We have also implemented a "computational window" which follows the detonation front in the calculation, so that we can study its propagation in three-dimensional systems on a long time scale.

Here, we use the model to confirm and complete the previous molecular-dynamics investigations of shock-induced detonations and, in particular, we study how the detonation wave structure is affected by the time required for molecules to react after they have been subjected to the leading shock.

II. MODEL FOR THE INTRAMOLECULAR STATE

Here, we extend our previous work[10] to consider a *three-dimensional* lattice composed of two-component molecules. The components of each molecule are designated N and C, each of which can represent a complicated atomic group. For instance, the C—N bond could represent the carbon-nitrogen bond in CH_3NO_2.

Previously, we represented the intramolecular bonds by a predissociative exothermic potential based on *ab initio* calculations of the excited state of the nitromethane molecule.[17] We know that this potential is much sharper than the intermolecular potentials connecting adjacent molecules because the intramolecular vibrational frequencies are approximately an order of magnitude higher than the intermolecular frequencies. Here, we take advantage of this disparity to represent intramolecular interactions and their coupling with the intermolecular motions by the model described below.

The sharpness of the intramolecular interaction potential means that the intramolecular bonds are much stronger than the intermolecular bonds. Consequently, while intermolecular bonds can be strongly compressed or stretched in the shock front, the length of intramolecular bonds does not change much as long as they are not broken. For this reason, we keep the intramolecular C—N bonds rigid until they break. During the calculation, the external forces on these rigid bonds are monitored and the internal state of the molecule is adjusted in response to the changing environment. Because the constraints are turned off or on depending on the internal state of the molecule, we call then *adaptive constraints.*

The advantages of this approach follow.

1. The equations describing intermolecular states can be separated from the calculation of intramolecular states. The strengths and other properties of the two types of interactions can be varied independently.

2. The coupling between intermolecular and intramolecular states can be specified and varied. For ex-

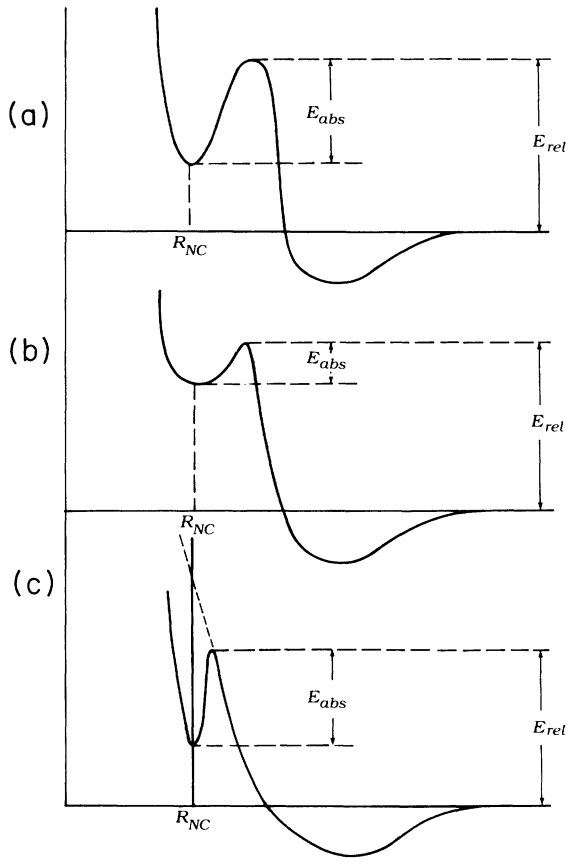

FIG. 1. Predissociative intramolecular interaction potential: (a) actual potential, (b) potential used in previous molecular-dynamics simulations of detonations (Refs. 12 and 13), and (c) potential corresponding to our predissociative-constraint model. E_{abs} is the energy absorbed by the molecules to reach before breaking and E_{rel} is the energy released upon breaking.

ample, exothermic and endothermic energy transfer between intermolecular and intramolecular modes can be modeled.

3. The level of complexity of the intramolecular model can vary. For example, semiclassical state-to-state transitions that model quantum effects can be introduced.

4. The numerical time step use to integrate the equations of motion, determined by the strength of the forces resolved, depends only on the intermolecular forces.

A. Predissociative rigid bonds

Figure 1 shows how the new model for predissociative rigid bonds is related to the models used in the molecular-dynamics simulations of detonations. In previous calculations[12,13] the sharp intramolecular potential was replaced by a smoother one in order to avoid the small time step that would have been required to integrate the equations of motion accurately. In the new approach, the imposed rigid bond is equivalent to replacing the sharp potential well by an infinitely sharp well. However, while the constraint is maintained, the effects of the intermolecular forces on the C—N bond are monitored and internal state parameters of the molecule are updated appropriately. When the internal state parameters reach preassigned values, the constraint forces are set to zero and the intermolecular C-N Lennard-Jones potential is switched on. As shown in Fig. 1, the amount of energy released in this process ($E_{\rm rel}$ in Fig. 1) depends on the parameters of the C-N Lennard-Jones potential and on the length $R_{\rm NC}$ of the constrained bond. The intermolecular-potential parameters are given in Table I. The energy release after dissociation as a function of $R_{\rm NC}$ is given in Table II. Most of the simulations used $R_{\rm NC}=2.84$ Å, corresponding to an energy release of 1 eV.

Consider a system of particles in which each particle moves in the force field of all the others. A constraint on any given particle, such as a fixed separation or fixed angular orientation, imposes a condition on the trajectory of that particle. The constraint force can be defined by the equations of motion describing the trajectory of a given particle i,

$$m_i\frac{d^2\mathbf{X}_i}{dt^2}=\mathbf{F}_i+\mathbf{F}^c(\mathbf{X}_i,\{\mathbf{X}_j\},\mathbf{V}_i,\{\mathbf{V}_j\},\mathbf{F}_i,\{\mathbf{F}_j\})\ . \quad (1)$$

In Eq. (1), $\mathbf{F}_i$ is the total force on particle i of mass m_i due to the other particles in the system, $\mathbf{F}^c$ is the force that maintains the constraint on particle i, and $\mathbf{X}_i$ and $\mathbf{V}_i$ are the position and velocity, respectively, of particle i, $\{\mathbf{X}_j\}$ and $\{\mathbf{V}_j\}$ are the sets of positions and velocities of the particles that are constrained with particle i, and $\mathbf{F}_j$ is the total force on each of the constrained particles $j\neq i$.

In the calculations presented here, the constraint between the two particles in a C—N bond is introduced as an additional intramolecular interaction $\delta\mathbf{F}_{ij}$ that is a function of the position, the velocity, the total force on each of the two interacting particles, and of parameters defining the internal state of the molecule through a *state function* $S(t)$. That is,

$$\delta\mathbf{F}_{ij}=\mathbf{F}^c(S(t),\mathbf{X}_i,\mathbf{X}_j,\mathbf{V}_i,\mathbf{V}_j,\mathbf{F}_i,\mathbf{F}_j)\ . \quad (2)$$

Because the coupling between intermolecular and intramolecular states is modeled on the intermolecular time scale, which is much larger than the intramolecular time scale, the value of $S(t)$ represents a cumulative effect or an average of many changes in the intramolecular state. The state function S is a continuous function that depends on intramolecular degrees of freedom and on molecular trajectories in a manner similar to that of a scattering or reaction cross section. We assume that the changes in the average total energy E of the molecule and the changes in $S(t)$ are related by

$$\frac{\partial S}{\partial t}\sim\frac{\partial E}{\partial t}\ . \quad (3)$$

The force for constraining the motion of two rigidly bound particles is[16,18]

$$\delta\mathbf{F}_{ij}^c=\frac{m_im_jl}{(m_i+m_j)(\delta t)^2}\left[1+\frac{l\cdot\Delta l}{l^2}\left[\frac{R_{\rm NC}^2}{l^2}+\frac{(l\cdot\Delta l)^2}{l^4}-\frac{(\Delta l)^2}{l^2}\right]^{1/2}\right], \quad (4)$$

where

$$\Delta l=(\mathbf{V}_j^{n-1/2}-\mathbf{V}_i^{n-1/2})\delta t+\left[\frac{\mathbf{F}_j^n}{m_j}-\frac{\mathbf{F}_i^n}{m_i}\right](\delta t)^2 \quad (5)$$

and

$$l=\mathbf{X}_j^n-\mathbf{X}_i^n\ . \quad (6)$$

In Eqs. (4) and (5), the superscripts n label the time step δt in the integration of the equations of motion that determine $\mathbf{X}$ and $\mathbf{V}$. The integration is performed with the leapfrog algorithm

TABLE I. Lennard-Jones intermolecular potential parameters.

Interaction	ϵ (eV)	σ (Å)
N-N	0.03	3.5636
C-C	0.006	4.00
N-C	0.009	3.8

TABLE II. Energy release after dissociation as a function of rigid bond distance $R_{\rm NC}$.

$R_{\rm NC}$ (Å)	Energy release (eV)
2.5	5.03
2.6	3.07
2.688	2.0064
2.749	1.5011
2.84	0.9789
2.9845	0.5001

$$\mathbf{X}_i^{n+1}=\mathbf{X}_i^n+\mathbf{V}_i^{n+1/2}\delta t \tag{7}$$

and

$$\mathbf{V}_i^{n+1/2}=\mathbf{V}_i^{n-1/2}+(\mathbf{F}_i^n+\delta\mathbf{F}_{ij}^n)\frac{\delta t}{m_i} . \tag{8}$$

A derivation of Eq. (4) starting with Eqs. (7) and (8) is given in Ref. 16 and 18.

It follows from Eq. (4) that the constraint force $\delta\mathbf{F}_{ij}^c$ is proportional to $(\mathbf{F}_i-\mathbf{F}_j)$, and consequently the intermolecular forces can be used to determine the integration time step. If $\delta\mathbf{F}_{ij}^c$ were either a function of the value of an intramolecular force, or a nonlinear function of $\mathbf{F}_i$ and $\mathbf{F}_j$ in a more general model, a smaller integration time step would be required.

We associate a *threshold* value $S_{\rm dis}$ with the state function S such that the condition $S(t)\geq S_{\rm dis}$ defines the dissociated state. The predissociative constraint force is defined by

$$\delta\mathbf{F}_{ij}=(\delta\mathbf{F}_{ij}^c)[1-U(S(t)-S_{\rm dis})] , \tag{9}$$

where $\delta\mathbf{F}_{ij}^c$ is given by Eq. (4) and $U(x)$ is the unit step function whose value is 1 for $x\geq 0$ and 0 for $x<0$. Thus, when $S(t)\geq S_{\rm dis}$, the constraint force is set equal to zero and the intermolecular Lennard-Jones interaction is switched on. It is important to note that angular momentum is conserved when the molecule makes a transition from the bound to dissociated state. The adaptive-constraints method could be extended to model bonds whose length can vary in time by changing $R_{\rm NC}$ in time.

B. The intramolecular state

The value of the state function $S(t)$ is obtained by monitoring the external stress to which a molecule is subjected and changing $S(t)$ accordingly. Because the force that is necessary to maintain a rigid bond is determined by the external forces on the molecule, the calculation of the constraint force provides the information needed to update $S(t)$. The impulse along the intramolecular bond due to intermolecular interactions during time step δt (Refs. 16 and 18) is

$$\Delta f_{ij}^n\delta t=\frac{m_i m_j(\boldsymbol{l}\cdot\Delta\boldsymbol{l})}{(m_i+m_j)(\delta t)l} . \tag{10}$$

We use this quantity to establish a criterion for assigning particular values to $S(t)$, according to

$$S(t+\delta t)=\begin{cases} S(t)+\Delta S_{\rm ex} & \text{if } |\Delta f_{ij}^n|\geq F_{\rm th} \text{ and } \Delta f_{ij}^n>0 \\ S(t)-\Delta S_{\rm dex} & \text{if } |\Delta f_{ij}^n|<F_{\rm th} \text{ and } \Delta f_{ij}^n>0 \\ S(t)-\Delta S_{\rm dex} & \text{if } \Delta f_{ij}^n<0 . \end{cases} \tag{11}$$

When Δf_{ij}^n is positive and its modulus exceeds a given threshold $F_{\rm th}$, $\Delta S_{\rm ex}$ is added to $S(t)$. This corresponds to an excitation of the C-N molecule under a high compression. If Δf_{ij}^n is below the threshold $F_{\rm th}$ or corresponds to expansion, spontaneous deexcitation of the molecule is allowed by subtracting $\Delta S_{\rm dex}$ from $S(t)$. Thus, $\Delta S_{\rm ex}$ is the change in $S(t)$ per time step for energy transfer from intermolecular modes to intramolecular modes, and $\Delta S_{\rm dex}$ is the change in $S(t)$ per time step for energy transfer from intramolecular modes to intermolecular modes. Here, the quantities $\Delta S_{\rm ex}$ and $\Delta S_{\rm dex}$ have been made integral multiples of each other. Thus the function S assumes discrete and equally spaced values between 0 and $S_{\rm dis}$. The threshold parameter $F_{\rm th}$ defines the sensitivity of the coupling between the internal and external states. A small value of $F_{\rm th}$ allows a weak external impulse to increase the value of the internal state function, and thus allows the molecules to dissociate in a weak external field.

Here a change in the intramolecular state occurs only when $\Delta f_{ij}^n>0$, which means that compression causes the electronic transitions leading to dissociation. This condition is physically realistic for molecules in the induction zone, the region between the shock front and reaction front. State transitions occurring for positive values of Δf_{ij}^n are consistent with assuming that a series of chemical processes occur at small internuclear separations. However, by allowing state changes when $\Delta f_{ij}^n<0$, we could consider the effects of expansion on the molecule.

Because $S(t)$ can increase at most by $\Delta S_{\rm ex}$ during a time step δt, the minimum time $t_{\rm min}$ for a molecule to dissociate is

$$t_{\rm min}=\delta t\frac{S_{\rm dis}}{\Delta S_{\rm ex}} . \tag{12}$$

However, since $S(t)$ may not increase at each time step if the molecule is not sufficiently compressed, and because spontaneous deexcitation is allowed, the actual time for a molecule to reach the dissociation threshold after the shock passes is generally longer than $t_{\rm min}$. The combination of the parameters $F_{\rm th}$, $\Delta S_{\rm ex}$, $\Delta S_{\rm dex}$, and $S_{\rm dis}$ determines the rate of energy transfer between the intramolecular and intermolecular states and the minimum time delay preceding molecular dissociation.

The condition for dissociation should correspond to a physically realistic response of the molecule to changes in the external intermolecular field occurring over time. The bond-breaking time should be at least on the order of one period of oscillation for intramolecular vibrational modes, e.g., $(1.5-3)\times 10^{-14}$ s. This is a lower bound on the time required for internal transitions leading to molecular dissociation. Changes in the internal state must be consistent with this time scale. In general, we expect the time for internal excitation leading to dissociation to be from two to ten periods of oscillation for vibrational modes.

The energy exchange between the intramolecular and the intermolecular motions depends on the force Δf_{ij}^n defined by Eq. (10). Because we define internal state parameters on the intermolecular time scale, changes in the internal state parameters represent continuous amounts of energy added to or absorbed from intermolecular modes. The energy transfer and $S(t)$ are discrete because they are represented by finite differences that are suitable for numerical modeling, and their values do not necessarily correspond to actual quantum transitions. Howev-

er, the model is designed in such a way that it could be extended to include actual quantum effects through semiclassical descriptions. It could also be extended to describe complex chemical interactions. For example, the state function S could be used to represent a *lumped* system so that the bond-breaking step could correspond to a considerably more complicated reaction pathway consisting of an endothermic dissociative process and a subsequent exothermic recombination of the dissociated groups.

C. The energy-transfer process

Because the variation of $S(t)$ corresponds to excitation or deexcitation of the C-N molecule, we must also include the corresponding energy transfer by adding or subtracting energy from the intermolecular motions in a way that is physically reasonable. The criterion for energy transfer should be based on values of S. Here we have adopted a relatively simple model for energy transfer in which a change in $S(t)$ is accompanied by either an addition to or a subtraction from the kinetic energy for the C-N system. When the value of S is increased, an amount of energy $\Delta E_{\rm ex}$ is subtracted from the system by rescaling the velocities of the atom groups C and N. Similarly, when $S(t)$ is decreased, an amount of energy $\Delta E_{\rm dex}$ is added to the system by the rescaling of velocities. To ensure energy conservation, $\Delta E_{\rm ex}$ and $\Delta E_{\rm dex}$ satisfy the condition

$$\frac{\Delta E_{\rm ex}}{\Delta S_{\rm ex}} = \frac{\Delta E_{\rm dex}}{\Delta S_{\rm dex}} , \tag{13}$$

which is a consequence of Eq. (3).

It follows from Eq. (13) that the total energy absorbed $E_{\rm abs}$ before dissociation of the C-N system [before $S(t)=S_{\rm dis}$] is given by

$$E_{\rm abs} = \Delta E_{\rm ex} \frac{S_{\rm dis}}{\Delta S_{\rm ex}} . \tag{14}$$

This energy corresponds to the energy $E_{\rm abs}$ shown if Fig. 1 and the total energy exchanged between the C-N molecule and the intermolecular motions is

$$E_{\rm tot} = E_{\rm rel} - E_{\rm abs} . \tag{15}$$

III. COMPUTING INTERPARTICLE FORCES AND TRACKING PARTICLES

Most of the computational cost in molecular-dynamics simulations is associated with calculating forces and tracking particle positions. This cost increases rapidly as the dimensions or number of particles in the system increase. For some types of molecular-dynamics simulations, important features of the system can be computed using as few as several hundred particles. For example, the equation of state or condensation levels can be computed for gas systems consisting of only 100 particles. However, a calculation of a system such as a shock or detonation in a crystal requires relatively large systems. For such calculations, it is necessary to have efficient methods of computing forces.

The detonation wave consists of different regions, each characterized by different densities and levels of order. For example, the regions making up a detonation in a given system could be defined as the unperturbed, unshocked crystal lattice comprised of well-defined unit cells; a dense, less-ordered reaction zone; and a product zone typically at gas densities. Tracking particles and computing forces should be optimized by taking into account the characteristics of the different regions of the system.

We have adapted the monotonic Lagrangian grid algorithm[14,15] (MLG) for tracking particle positions and for computing forces. In a MLG, adjacent particles in space have grid indices that are also adjacent in computer memory. Because it is always possible to assign linearly ordered grid indices to a set of randomly located particles in three-dimensional (3D) space, such an indexing scheme can be used to construct a MLG. For example, to each particle position (X,Y,Z), MLG coordinates (i,j,k) can be assigned according to the monotonicity conditions: $X_i \le X_{i+1}$, $Y_j \le Y_{j+1}$, and $Z_k \le Z_{k+1}$. Grid coordinates (i,j,k) satisfying these monotonicity conditions are in *MLG order*. Particles which have their position coordinates in MLG order can be tracked efficiently. In addition, the MLG can be used to index velocities and other attributes of particles such as particle-type labels or flags. The MLG indexing is compact in the sense that the memory locations required for indexing particle positions equals the number of particles in the system. For a given particle, it is not necessary to search grid locations to find its neighbors. Further, because all grid locations contain particles, it is not necessary to sweep through a MLG to determine which locations are occupied.

For particles which have their position coordinates in MLG order, forces between neighbors can be computed efficiently by using a maximum index offset N_c, rather than some condition associated with bounds on the separation of particles in space. The index N_c is selected so that no two particles can be close in space and yet have differences in their grid indices greater than N_c. We define a *neighbor template* by a main grid location and a fixed number of close locations defined by N_c. The size of the neighbor template will depend on the particle density and the relative level of order in the system. References 14 and 15 discuss the importance of the size of the template and discuss methods of optimizing and vectorizing MLG algorithms.

Because the system of particles is continually changing its configuration, it is necessary to continually update the MLG to maintain the MLG order. The MLG can be efficiently updated by locally comparing and then swapping MLG coordinate indices to maintain MLG order. This method is highly efficient for sorting a sequence which is slightly out of order, as is the case for a MLG indexing particle positions in a molecular-dynamics simulation. The requirements of accuracy and stability for the numerical integration of the equations of motion limit time-step size, permitting only a slight disordering of a MLG at each time step.

IV. RESULTS

A. The crystal model

The first step in developing the crystal model is to use the rigid C-N molecules to construct a three-dimensional lattice that is in a stable minimum-energy state. In our model, the molecules are connected by Lennard-Jones potentials that are efficient to use in force calculations. Given the length of the rigid C—N bond and the parameters of the intermolecular potentials, a stable lattice is obtained by an energy minimization procedure. We start the procedure with a nearly stable lattice configuration estimated from the potential minima of the neighbor field, and then let the lattice relax by damping the equations of motions. The optimum damping parameter has been determined empirically. After a time the damped calculation is stopped, the central unit cell in the system is chosen as the basic configuration for another lattice, and this new lattice is allowed to relax. This procedure is repeated until the newest lattice remains stable in free space when there is no damping applied.

We found that we could construct two stable lattices with significantly different symmetry properties. These lattices, subsequently referred to as type 1 and type 2, are shown schematically in Figs. 2 and 3. The type-1 lattice has one C-N molecule in each unit cell, and the type-2 lattice has two molecules in a unit cell. The existence of two stable lattices for a given geometry of C-N molecules and given interaction potentials is not surprising because it is known that there are two stable lattice configurations in a crystal consisting of homonuclear diatomic molecules such as N_2.[19] For the lattice we are considering here, which consists of heteronuclear diatomic molecules, there could be more than two. The type-2 lattice configuration has a lower energy than the type-1 lattice configuration.

The masses of the N and C atoms are 47 and 15 atomic mass units, respectively, consistent with the masses of NO_2 and CH_3 groups.[10] Most of the calculations were performed with the Lennard-Jones parameters given in

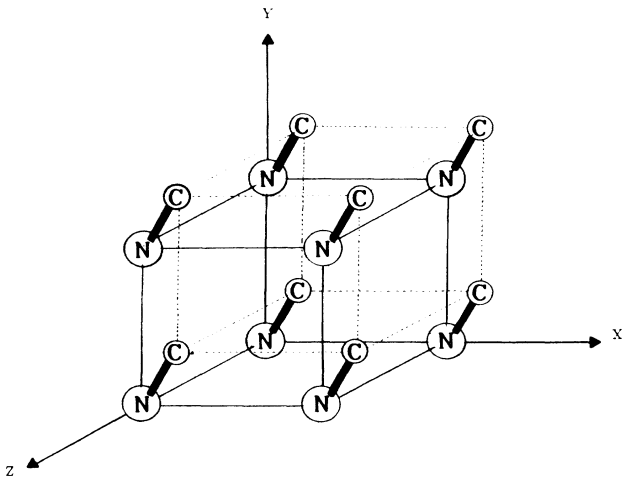

FIG. 2. Type-1 stable-lattice configuration.

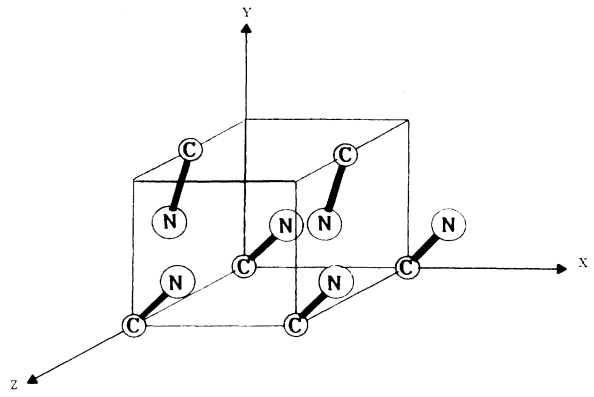

FIG. 3. Type-2 stable-lattice configuration.

Table I for the three intermolecular potentials, N-N, N-C, and C-C, which are similar to the Lennard-Jones parameters used in our previous model.[10] The same parameters used in the calculations whether or not the interacting particles are bound to other particles or are fragments of dissociated pairs. These parameters are reasonable for intermolecular potentials in a typical energetic crystal rather than being an exact specification of any particular crystal lattice. They produce frequencies of the acoustic lattice modes which are consistent with the values expected for a molecular crystal. In addition, the ratio of the force constants defining the strong N-N interactions to the force constants defining the weak C-C interactions is consistent with the values deduced from atom-atom interaction potentials for NO_2 and CH_3 groups.[20] Finally, the speed of sound in the lattice is approximately 2200 m/s, which is reasonable for a crystal having a relatively rigid sublattice. The geometric parameters of the type-1 and type-2 lattices, obtained with the interaction potentials listed in Table I, are given in Table III.

In some of the calculations, a second set of Lennard-Jones parameters has been used to investigate the effect of interparticle bond strength. In this set, the strong bonds are between the light C groups, while the weak bonds connect the heavier N groups. Table IV lists these parameters, and the geometric characteristics of the type-2 lattice that results.

Typical calculations contained from 896 to 3600 lattice cells. The systems simulated are periodic in the X and Y directions. The detonation always propagates in the Z direction. Lattice cells may be subtracted and added at the left and right boundaries in the Z direction while keeping the number of particles in the system constant. This addition and subtraction is used to define a moving window that follows the detonation front after the detonation has reached a stable self-sustaining state. A typical calculation for one set of parameters requires 20–60 min of Cray Research, Inc. X-MP 148 supercomputer time.

To simulate the shock initiation process in our calculations, a constant force is applied to the N and C particles in the leftmost plane of cells in the Z direction during a limited time, and then this left Z boundary is left free.

TABLE III. Lattice parameters and relative atomic coordinates for equilibrium configurations.

Type-1 lattice (1 C-N molecule per unit cell)
Lattice parameters: $a=4.61$ Å, $b=4.61$ Å, $c=4.61$ Å
Length of N—C bond: 2.84 Å

Atom number	Group type	Relative coordinates		
		X	Y	Z
1	N	0	0	0
2	C	0.355 68	0.355 68	0.355 68

Type-2 lattice (2 C—N molecules per unit cell)
Lattice parameters: $a=4.573$ Å, $b=4.573$ Å, $c=8.073$ Å
Length of C—N bond: 2.84 Å

Atom number	Group type	Relative coordinates		
		X	Y	Z
1	C	0	0	0
2	N	0.3375	0.3375	0.2249
3	C	0.8358	0.8358	0.5000
4	N	0.4983	0.4983	0.7249

The window is moved is such a way that the right Z boundary always corresponds to a portion of the original crystal that has not yet been reached by the leading shock front. In these calculations we have focused our attention on the structure of a steady detonation and we have not attempted to study the microscopic basis of the shock initiation, which might require investigations on a much longer time scale.

B. Effects of lattice geometry

In order to discuss the results of the simulations, it is necessary to adopt a microscopic definition of a shock front and a reaction front. We define the leading shock front of the detonation as that location where the kinetic energy of the particles is greater than that value corresponding to the temperature of the undisturbed lattice. We define the reaction front as that position behind the leading shock where a bond breaks, or equivalently, where $S(t)=S_{\text{dis}}$ for a molecule in the lattice. Figure 4 shows the propagation of the detonation in the type-1 and type-2 lattices. The thin solid line indicates the position of the shock front and the heavy bars indicate the position of the reaction front. In both simulations, the energy release after dissociation, E_{rel}, is 0.98 eV, the energy absorbed for breaking, E_{abs}, is 0.08 eV, and the minimum time for bond breaking, t_{min}, is 2×10^{-15} s. However, the characteristics of a propagating detonation are significantly different in the type-1 and type-2 lattices.

The striking feature of the detonation in the type-1 lattice is the regular oscillation of the induction zone, defined here as the distance between the shock front and the reaction front. This effect can be explained on the basis of the differences between the type-1 and type-2 lattice geometries. The type-2 lattice has a symmetry plane parallel to the Z axis, which is the direction of propagation of the detonation, and the type-1 lattice has no such symmetry plane. Because of this symmetry, the average interparticle force is along Z in the type-2 lattice, whereas it is oblique to the Z direction in the type-1 lattice. Thus transverse coupling is stronger in the type-1 lattice, and transverse motions are more likely.

TABLE IV. Lattice and potential parameters and relative atomic coordinates of type-2 lattice with strong bonds between light-atom groups.

Lennard-Jones potential parameters

Interaction	ϵ (eV)	σ (Å)
N-N	0.006	4.0
C-N	0.03	3.5636
N-N	0.009	3.8

Lattice parameters: $a=4.6$ Å, $b=4.6$ Å, $c=8.6$ Å
Length of C—N bond: 2.84 Å

Atom number	Group type	Relative coordinates		
		X	Y	Z
1	C	0	0	0
2	N	0.32	0.32	0.2246
3	C	0.8	0.8	0.5
4	N	0.48	0.48	0.7246

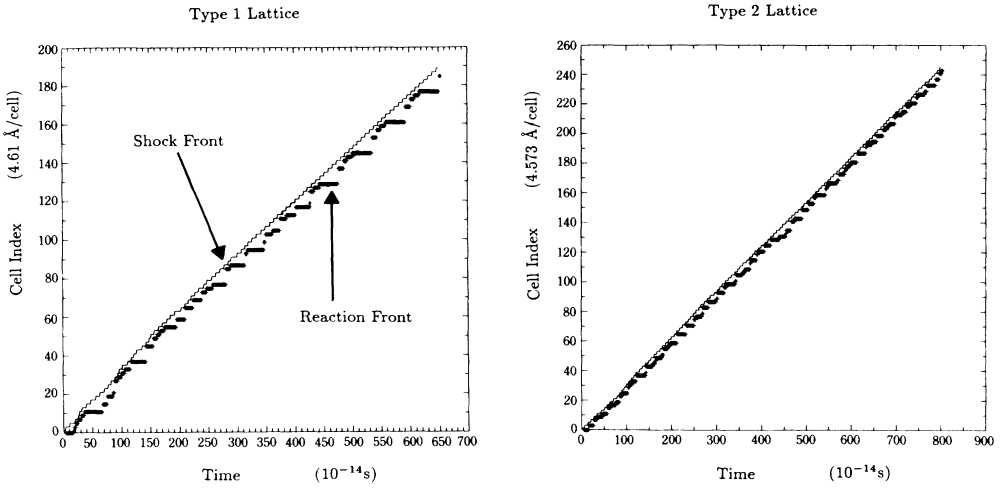

FIG. 4. Relationship between shock front and reaction front in type-1 and type-2 lattices. The thin line indicates the position of the shock front and the thick line indicates the position of the reaction front.

We have correlated the oscillations in the size of the induction zone to the interaction of transverse waves with the periodic boundaries of the computational domain by comparing the period of oscillation in lattices with 8×8 and 12×12 cells. For eight cells in the transverse direction, the period is 5.75×10^{-13} s; for 12 cells, it is 8.65×10^{-13} s. The period is therefore directly proportional to the transverse dimension of the lattice. It corresponds to a speed of 6390 m/s for the transverse waves, which is a reasonable value for a shock wave in a crystal.

The presence of transverse waves in asymmetric lattices was also seen in simulations in a two-dimensional system.[11] The asymmetric lattice, which is similar to a two-dimensional projection of the type-1 lattice described here, shows oblique patterns in the induction zone and a shock front which makes an angle of 45° with the Z direction. The symmetric lattice does not show oblique patterns but rather a wavy front that stays on average perpendicular to the Z direction. However, in the two-dimensional model, transverse waves appear only in systems with more than 20 cells in the transverse direction, whereas they are found in three-dimensional systems which are only eight cells wide. In a three-dimensional system, we expect all transverse motions to be more important because there are two transverse degrees of freedom for each longitudinal one. The results, for both the two-dimensional and three-dimensional systems, support the conclusion that a planar detonation front perpendicular to the direction of the propagation of the detonation does not persist in an asymmetric lattice structure.

The average detonation speed is 12 562 m/s in the type-1 lattice and 13 188 m/s in the type-2 lattice. The presence of transverse waves in the asymmetric lattice reduces the average detonation speed because energy removed from the longitudinal motions along Z cannot be used to drive the shock along Z. These detonation velocities (Mach 5–6) are high compared to the estimated speed of sound, 2250 m/s. However, the order of magnitude is consistent with a short $t_{\min}$ and a small E_{abs}.

C. Effects of interparticle bond strength

Previous two-dimensional simulations[10,11] showed that a massive and strongly bound sublattice is necessary for a stable detonation to propagate. We examined this in the three-dimensional model by comparing a detonation propagating in a type-2 lattice with a massive rigid sublattice (Table III) to a detonation in a type-2 lattice with a light rigid sublattice (Table IV). In both cases, the detonation propagates if the energy release after molecular dissociation is sufficiently large. However, it is much more difficult to obtain a detonation when the rigid sublattice consists of the light atoms. For an energy release of 0.98 eV, a minimum delay for bond breaking of 10^{-13} s and an excitation impulse applied on the leftmost lattice plane for 5×10^{-14} s, it was necessary to give the leftmost lattice plane an initial velocity of 25 000 m/s in order to initiate a detonation in the crystal with a light rigid sublattice. However, in the case of the crystal with a heavy rigid sublattice, a stable detonation could be achieved with an initial velocity of only 15 000 m/s.

D. Effects of minimum delay for molecular dissociation

The value of $t_{\min}$, defined by Eq. (12), can be varied independently to investigate the dependence of detonation structure on the characteristic response time of potentially dissociative molecules. In previous calculations,[10–13] the delay between the time when the shock front reached a given molecule and the dissociation of that molecule was determined by the classical model for the metastable bond. Although it was not explicitly computed, this delay was short because the average distance between the shock front and reaction front was 2–5 cells, a distance that the shock wave crosses in 6.0×10^{-15} to 1.5×10^{-14} s at the detonation speed. This is on the time scale of intramolecular oscillations ($\approx1.6\times10^{-14}$ s per period), implying that bond breaking was due to purely mechanical effects. Bond breaking on such a short time scale does not take into account the time that may be necessary to

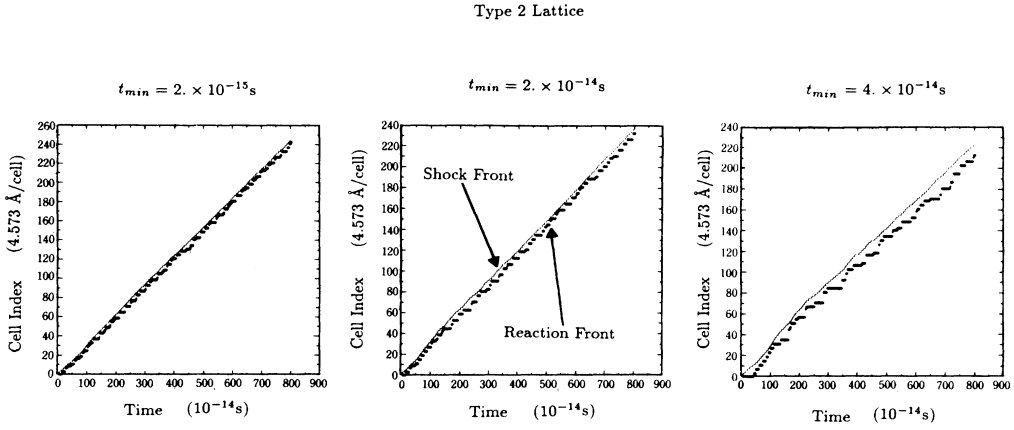

FIG. 5. Relationship between shock front and reaction front as a function of the minimum delay time t_{min} for molecular dissociation.

excite a molecule from its associative electronic ground state to a predissociative state, an effect that the mechanical model for bonding did not include. The current model permits us to specify delay times for molecular dissociation and energy release which are more typical of chemical reactions.

We investigated minimum time delays in the range 2.0×10^{-15} s (very fast bond breaking) to 10^{-13} s (slow bond breaking corresponding to about six oscillation periods). Figure 5 shows the propagation of a detonation in the type-2 lattice specified by the parameters in Table IV. Similar results are obtained for the type-2 lattice specified by Table III. Figure 5 suggests several interesting properties of the detonation structure. First, the structures associated with the different zones making up a reaction front are qualitatively similar when t_{min} changes. The detonation propagates for all three cases, i.e., $t_{min}=2.0\times10^{-15}$, 2.0×10^{-14}, and 4.0×10^{-14} s, even though t_{min} varies more than one order of magnitude. Second, as t_{min} increases, the average distance between the shock and reaction front increases and the reaction front becomes progressively more distorted or irregular. Third, the detonation speed decreases as t_{min} increases.

Figure 6 shows how the detonation speed varies with t_{min} for a detonation propagating in the type-2 lattice defined by Table IV and an energy release and absorption of 0.978 and 0.08 eV, respectively. Here, there is a decrease of more than 20% when t_{min} increases from 2.0×10^{-15} to 10^{-13} s. The decrease in detonation speed with increasing t_{min} can be explained by considering the microscopic energy-release process. When t_{min} is large, bonds break far from the shock front and thus the energy released is not transmitted efficiently to the shock front. Instead, part of the energy goes into transverse modes or random thermal motion.

The dependence of detonation speed on t_{min} is not consistent with the classical theory of detonations[21] in which a detonation speed is calculated from energy, momentum, and mass conservation between two planes, one situated before the shock front and one situated well after the reaction zone. This classical detonation theory does not include information on the details of chemical processes such as the delay time for molecular dissociation. We do not expect, however, that a complete description of microscale detonation structure can be provided by the classical detonation theory since, at the microscopic level, the equilibrium conditions required for the application of this theory may not be satisfied.

Figure 7 shows the spatial distribution of the kinetic energy in the detonation wave for two extreme values of t_{min}, 2.0×10^{-15} and 1.0×10^{-13} s. Although there are quantative differences between these pictures, the main features are preserved. First, there is a very sharp rise in kinetic energy at the very narrow shock front, which is 10 Å or two intermolecular distances wide. This rise is followed by a sharp decrease and then another rise due to molecular dissociation. Even with a small t_{min}, there is a sharp decrease in kinetic energy behind the shock front,

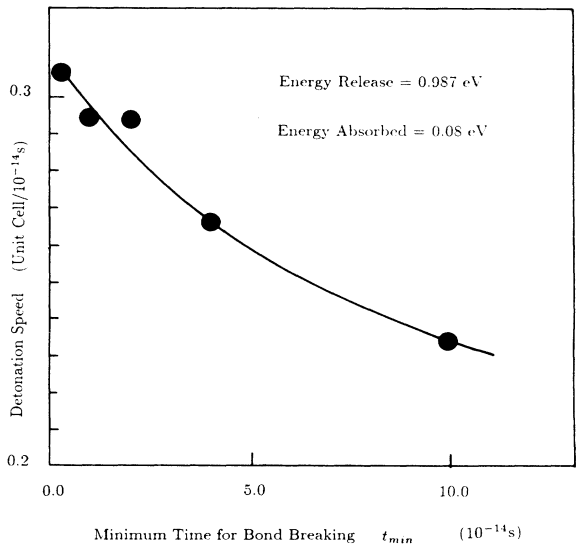

FIG. 6. Detonation speed in type-2 lattice as a function of t_{min}.

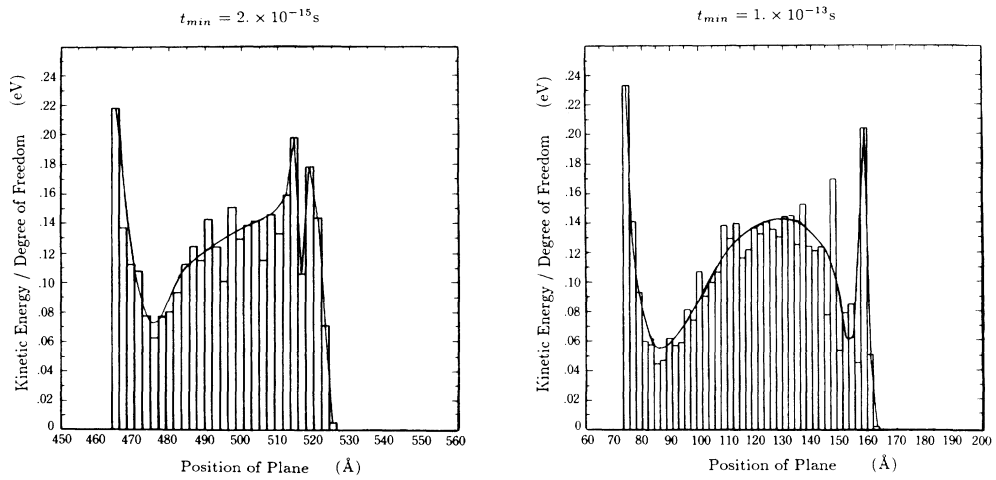

FIG. 7. Spatial distribution of kinetic energy in detonation corresponding to different values of $t_{\min}$. Each box corresponds to an average of the kinetic energy of the particles in one lattice plane in the (X, Y) directions.

indicating that this structure is not a random fluctuation. This decrease could result from energy absorption before bond breaking, although this is unlikely because the energy absorption was only 0.08 eV per molecule in this case. Finally, the kinetic energy increase shown in Fig. 7 near the window boundary is due to the free left boundary which causes a rarefaction wave. This is discussed further below.

E. Effect of energy transfer before molecular dissociation

The effect of varying E_{rel} and E_{abs} are summarized in Table V. We have found that the detonation fails below a minimum value in the global energy release. Thus *slow* detonations with small energy release should not be expected. This result is consistent with our two-dimensional results and with commonly understood macroscopic properties of detonations.[21] The detonation fails when the energy release is reduced by either reducing the dissociation energy or by increasing the energy absorbed. However, we have not yet tested whether the failure depends only on the global energy release. It is likely that the way the energy is distributed between dissociation energy and E_{abs} is of some importance.

When E_{abs} becomes large but the dissociation energy is sufficient to form a stable detonation, the distance between the shock front and the reaction front oscillates, as shown in Fig. 8. These oscillations are different from those generated by transverse waves in the asymmetric type-1 lattice. Here, they appear in a type-2 lattice, which has a symmetry glide plane parallel to the Z axis, and because their period is much larger than that of the oscillations due to tansverse waves in the type-1 lattice. The origin of these oscillations is currently under investigation.

TABLE V. Effect of energy release and energy absorption on the detonation speed.

Lattice	Energy released (eV)	Energy absorbed (eV)	Global energy (eV)	$t_{\min}$ (s)	Detonation speed (cell/10^{-14} s)
Type 2 (Table IV)	0.978	0.08	0.898	1×10^{-14}	0.2933
Type 2 (Table IV)	0.978	0.08	0.898	1×10^{-13}	0.236
Type 2 (Table III)	0.978	0.08	0.898	1×10^{-13}	0.305
Type 2 (Table IV)	0.50	0.08	0.42	1×10^{-14}	Failure
Type 2 (Table IV)	0.50	0.08	0.42	1×10^{-13}	Failure
Type 2 (Table IV)	0.978	0.25	0.728	1×10^{-14}	Failure
Type 2 (Table IV)	1.227	0.25	0.977	1×10^{-14}	0.245
Type 2 (Table III)	1.366	0.25	1.116	1×10^{-14}	0.3067

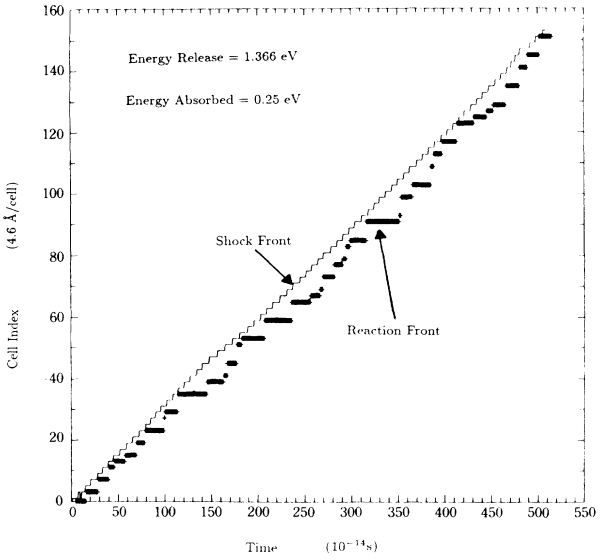

FIG. 8. Relationship between shock front and reaction front in type-2 lattice for large E_{abs}.

F. Effects of size of the computational window

Because each molecular-dynamics simulation is so computer intensive, it is important to determine the minimum size of a system required to resolve and study a particular detonation structure. In general, a molecular-dynamics calculation samples a small part of a larger system. A detonation, however, even on the microscale, can have structures with characteristic lengths extending over many hundreds of molecules. Selecting a particular size for a model system, what we call a computational window, imposes a length scale that is a function of the size of the model system. The model may then be too small to show the properties of the larger system that we wish to investigate, or may impose constraints that alter the properties that we do see.

An important consideration in selecting an appropriate computational window is the time scale for the transmission of information between the different regions of a detonation. In the simulations described here, we are interested in the relationship between the shock front and reaction front, and how this relationship depends on the lattice geometry and the time for molecular dissociation. Thus, in order to determine an appropriate size of the computational window, we must determine the effective size of the reaction zone and how large is the domain in the reaction zone which affects the structure of the reaction front.

In the simulations, the typical window size was $10\times10\times60$ particles ($10\times10\times30$ cells). We investigated the effect of window size in systems with a large t_{min}, 1.0×10^{-13} s, for which the reaction zone is large. Therefore the effect of window size in these systems should be sufficient for determining the appropriate window size for the systems where $t_{min}<1.0\times10^{-13}$ s. Figure 9 shows the distribution of kinetic energy in the detonation after 2.5×10^{-12} s for two different calculations with $t_{min}=1.0\times10^{-13}$ s; one with a sampling window of $8\times8\times56$ particles and the other with a sampling window of $10\times10\times100$ particles. The position of the shock front is exactly the same in both calculations. Moreover, the distribution of the kinetic energy in the reaction zone is the same in both calculations in a domain extending to about 90 Å large behind the leading shock front. Then, there is an increase in kinetic energy that is farther from the shock in the larger window. This increase is due to a rarefaction wave caused by the free left boundary. However, the simulations show that this rarefaction wave *does not extend noticeably into the system* because it propagates slower than the leading shock front. In a solid, the detonation wave is not only a pressure wave but it causes also a phase change in which the material goes from solid

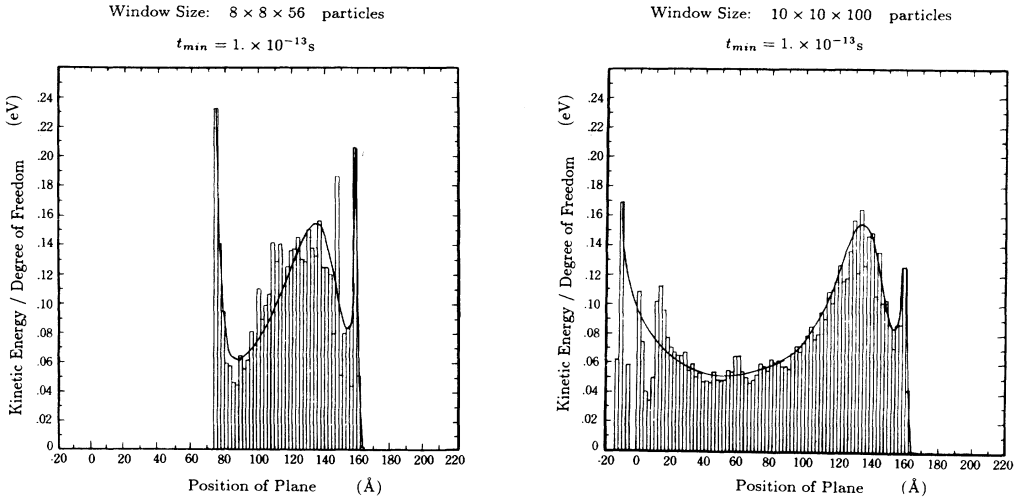

FIG. 9. Spatial distribution of kinetic energy in detonation corresponding to different sampling windows.

to fluid. Consequently, the nature of the propagation of sound waves changes in the different regions of the detonation wave. In the solid phase, they propagate at high speed as vibrations of the lattice whereas in the gas phase behind the shock front they are transmitted at lower speed by the atomic collisions. This difference in the mode of wave propagation may explain why only a limited region behind the shock affects the shock front and why the rarefaction wave cannot overtake the front.

V. DISCUSSION AND CONCLUSION

In this paper we have introduced an approach that extends the usual techniques of molecular-dynamics simulations of detonations by separating the intermolecular motions, treated in the conventional way, from the intramolecular state described by a model. We have tested this new approach by comparing its results with those of previous two-dimensional simulations. In addition, the greater efficiency of the new simulation technique has allowed us to consider a three-dimensional model. We then used the additional flexibility of the model to investigate the effects of the characteristic response time of potentially dissociative molecules subjected to the stress field of the leading shock front.

The general agreement between our previous two-dimensional simulations and the present three-dimensional calculations with a different model for the intramolecular states shows that the results are not model dependent. This has given us confidence in the approach using molecular dynamics for analyzing the microscopic features of detonations. The present calculations have confirmed the following points.

(i) The shock front is sharp on the atomic scale. There are even structures within the shock with a width of two unit cells which preserve their shape as the front propagates in the lattice. The usual gas-phase conditions, in which the shock width is determined by the mean free paths of molecules do not apply in solids.

(ii) The detonation wave is a partially coherent structure, that is, it propagates with a well-defined structure with longitudinal and transverse fluctuations superimposed.

(iii) The crystal structure has a strong influence on the characteristics of a detonation. In particular, for a detonation to propagate easily in a lattice, the two sublattices linked by dissociative bonds must be significantly different from each other. One must be massive and strongly bonded, and the other one must be light and weakly bonded.

(iv) The detonation speed is a characteristic of the lattice and not of the initial impulse.

Moreover, it was important to extend our previous calculations to three dimensions because they had shown the large role of transverse motions in determining the detonation speed and whether a stable detonation wave can even exist. The new simulations show that although the propagation of a detonation in a three-dimensional model is similar to that in a two-dimensional one, there are some important differences.

(i) As expected, the transverse motions play a larger role in three dimensions than in two dimensions. Although the periodic boundary conditions and the limited size of the system in the transverse directions tend to stabilize a planar detonation front perpendicular to the direction of the propagation, the front becomes oblique by forming transverse waves for much smaller systems in three dimensions than in two dimensions. In addition, the three-dimensional simulations do not show the same perfectly coherent state, almost without transverse motions, that appeared in two dimensions immediately after the initiation, before transition into the steady detonation.

(ii) There are new results in three dimensions due to the existence of different stable crystal structures. In some cases, the leading front can promote a transition from one structure to the other. Although we have not investigated in detail the role of this shock-induced phase transition, this may be an interesting feature because the transition is accompanied by a change in the potential energy of the crystal that may promote or inhibit a detonation.

By separating intramolecular states from intermolecular motions, we have been able to investigate the role of the minimum delay time that molecules in a predissociative state need to break. The results show that the qualitative structure of the detonation wave is preserved when the minimum delay for breaking increases by more than one order of magnitude. However, this variation affects the detonation by changing the detonation velocity and increasing the size of the induction zone. This effect, known also from hydrodynamic simulations of detonations in fluids,[1] is not included in the standard theory of detonations.[21]

The model that we have used here for the intramolecular states is rather simple, but is designed so that it can easily be extended to include, for example, quantum effects in the intramolecular state through a semiclassical treatment. Consequently, this approach provides a way to avoid the purely mechanical description of chemical reactions in molecular-dynamics simulations. The next step is to introduce several steps in the chemistry, including endothermic dissociation and exothermic recombination of the species.

Indeed, any approach that uses a model must be tested for possible model-dependent results. However, defining a model at the molecular level that reproduces the experimental features of detonations in solids is a step toward a theoretical understanding of these detonations on a microscopic scale. In that sense, our approach is similar to the macroscopic simulations of detonations in fluids which combine the equations of hydrodynamics with a model for the chemistry at the same macroscopic scale. Here we combine the microscopic equations describing the dynamics of atoms with a model for the chemical reactions at the same microscopic scale. In addition to providing information on the appropriate microscopic model for the chemistry in a detonation wave, using a model for the intramolecular states allows faster simulations so that larger systems can be studied for a longer time. We believe that this approach will eventually be used to bridge the gap between our understanding of detonations at macroscopic and microscopic scales.

ACKNOWLEDGMENTS

This work was supported by the Physics Division of the U.S. Office of Naval Research, by the Naval Research Laboratory, and by the Département de Recherches et d'Etude Techniques (France). We would like to acknowledge the continued support of Dr. Robert Junker and discussions with Dr. Robert Wyat and Dr. Herschel Rabitz. We would like to thank particularly Dr. Michael Page and Dr. Donald Tsai for their very useful comments. We would especially like to acknowledge the continuous help and encouragement provided by Professor Simone Odiot during the entire project.

*Permanent address: Laboratoire d'Optique du Réseau Cristallin, Faculté des Sciences, Université de Dijon, 6 boulevard Gabriel, 21100 Dijon, France.

[1]*Approches Microscopique et Macroscopique des Détonations,* edited by S. Odiot [J. Phys. (Paris) Colloq. C **4**, (1987)].

[2]H. N. Presles, M. Hallouin, and P. Harris, in *Approches Microscopique et Macroscopique des Détonations,* edited by S. Odiot [J. Phys. (Paris) Colloq. C **4**, 127 (1987)].

[3]N. Flytzanis, St. Pnevmatikos, and M. Peyrard (unpublished).

[4]D. H. Tsai and R. A. MacDonald, Phys. Rev. B **14**, 4714 (1976).

[5]J. Tasi, J. Appl. Phys. **51**, 5804 (1980); **51**, 5816 (1980).

[6]J. H. Batteh and J. D. Powell, Phys. Rev. B **20**, 1398 (1979).

[7]J. H. Batteh and J. D. Powell, J. Appl. Phys. **49**, 3933 (1978).

[8]A. M. Karo, J. R. Hardy, and F. E. Walker, Acta Astronaut. **5**, 1041 (1978).

[9]A. M. Karo, F. E. Walker, T. M. DeBoni, and J. R. Hardy, in *Proceedings of the 9th International Colloquium on the Dynamics of Energetic and Reactive Systems,* edited by J. R. Bowen, N. Manson, A. K. Oppenheim, and R. I. Soloukin (American Institute of Aeronautics and Astronautics, New York, 1984).

[10]M. Peyrard, S. Odiot, E. Oran, J. Boris, and J. Schnur, Phys. Rev. B **33**, 2350 (1986).

[11]M. Peyrard, S. Odiot, and M. Blain, J. de Chim. Phys. (to be published).

[12]D. H. Tsai and S. F. Trevino, J. Chem. Phys. **81**, 5636 (1984).

[13]S. F. Trevino and D. H. Tsai, in *Proceedings of the Eighth (International) Symposium on Detonations, Albuquerque, N. M., 1985* (Naval Surface Weapons Center, White Oak, Silver Spring, MD, 1985).

[14]J. Boris, J. Comput. Phys. **66**, 1 (1986).

[15]S. G. Lambrakos and J. P Boris, J. Comput. Phys. **73**, 2546 (1987).

[16]S. G. Lambrakos, J. P. Boris, E. S. Oran, I. Chandrasekar, and M. Nagumo (unpublished).

[17]C. Mijoule, S. Odiot, S. Fliszar, and J. M. Schnur, J. Mol. Struct. **149**, 311 (1987).

[18]S. G. Lambrakos, J. P. Boris, R. H. Guirguis, M. Page, and E. S. Oran (unpublished).

[19]*van der Waals Systems,* edited by F. L. Boschke (Springer-Verlag, Berlin, 1980).

[20]M. Peyrard, S. Odiot, E. Lavenir, and J. M. Schnur, J. Appl. Phys. **57**, 2626 (1985).

[21]W. Ficket and W. C. Davis, *Detonation* (University of California Press, Berkeley, 1979).